A review of progress on nano-aperture VCSEL

Invited Paper

Zhilong Rao, Sonny Vo, and James S. Harris

Solid State and Photonics Laboratory, Stanford University, Stanford, California, 94305, USA

This paper reviews the progress on nano-aperture vertical-cavity surface-emitting lasers (VCSELs). The design, fabrication, and polarization control of nano-aperture VCSELs are reviewed. With the nano-aperture evolving from conventional circular and square aperture to unique C-shaped, H-shaped, I-shaped, and bowtie-shaped aperture, both the near-field intensity and near-field beam confinement from nano-aperture VCSELs are significantly improved. As a high-intensity compact light source with sub-100-nm spot size, nano-aperture VCSELs are promising to realize many new near-field optical systems and applications.

1. Introduction

The technological promises of nano-aperture vertical-cavity surface-emitting lasers (VSCELs) range from ultrahigh-density near-field optical-data storage to improvements in microscopy and ultrahigh-resolution imaging to the study of single molecule manipulation, fluorescence and spectroscopy, and as a compact light source for future nanophotonic integrated circuits. Presently, conventional storage media such as compact disks, digital video disk, and blue ray disks use far-field optics. As such, the optical diffraction limit sets an upper bound on the optical storage density,

$$R = \frac{0.61\lambda}{\text{NA}}, \tag{1}$$

where R is the ideal resolution given the wavelength, λ, and the numerical aperture of the lens system, NA $= n \cdot \sin\theta_c$.

Partovi *et al.* first demonstrated the data recording and reading with a 250-nm-square-aperture nano-aperture laser based on a 980-nm wavelength edge emitting laser (EEL). A power output greater than 1 mW with a small output beam size ranging from $50 - 300$ nm were realized. This suggests that recording data with a density greater than 500 Gb/in^2 will be possible given better beam confinement and higher power intensity[1]. VCSELs are better candidates than EEL in these applications since they can be processed and tested on a wafer scale. Also, data transfer rates can be greatly increased by producing VCSELs in linear or two-dimensional (2D) arrays[2].

Thornton and Hesselink first proposed the idea of nano-aperture VCSELs[3]. To develop a nano-aperture VCSEL, the easiest way is to build it on the foundation of conventional VCSEL. For example, one can deposit a SiO$_2$ film and then an Au film on top of a conventional VCSEL. A nano-aperture VCSEL can be produced by opening a nano-aperture using a focused ion beam (FIB) on the Au film. The necessity of using the SiO$_2$ film will be discussed later. Figure 1 shows the main part of the structure of such a nano-aperture VCSEL based on a conventional VCSEL coated with SiO$_2$ and an Au film.

A major short-coming with this nano-aperture VCSEL structure is that the reflectivity of the top mirror in a conventional VCSEL is very high (typically about 99.5%). As a result, the power output through the top mirror, namely the intensity of light incident onto the nano-aperture, is very low compared to the intensity inside the laser cavity. Thus, the structure of the conventional VCSEL requires revision to increase the output power.

There are several possible approaches to improve the quantum efficiency, and hence, the power output from the nano-aperture VCSEL, as given by

$$P_{\text{out}} = \frac{\hbar\omega}{q}\eta \cdot (I - I_{\text{th}}), \tag{2}$$

where ω is the angular lasing frequency, q is the electron charge, η is the quantum efficiency, I is the injection current, and I_{th} is the lasing threshold current. The first method, initially proposed by Thornton *et al.* was to increase the intensity incident onto the nano-aperture by reducing the number of distributed Bragg reflector (DBR) pairs in the top mirror to enhance transmission[3]. The second method was to decrease the optical mode area by using a smaller oxide aperture to confine the optical mode. A third method was to reduce the total loss by using the oxide aperture to reduce optical scattering loss.
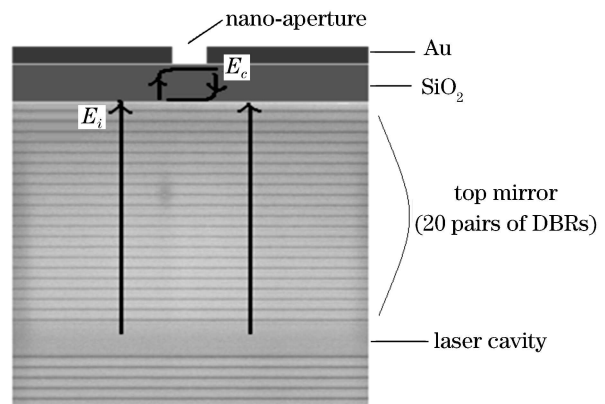

Fig. 1. Schematic structure of nano-aperture VCSEL based on a conventional VCSEL.

2. Nano-apertures: from simulations to experiments

Shinada *et al.* first demonstrated a micro-aperture VCSEL with a 400-nm square aperture, but only obtained a very weak output power density[4]. Improvements were made by using closely spaced double circular apertures[5,6] or a circular aperture with a metal particle situated in the center[7]. However, the near-field optical intensities from these nano-aperture VCSELs were still not high enough for optical recording and the near-field spot sizes were relatively large.

From a theoretical perspective, the power transmission through a conventional square or circular aperture decreases as the fourth power of the aperture size as the aperture becomes much smaller than the wavelength of the optical source[8]. This significantly limits the output intensity from nano-aperture lasers when the aperture size is decreased in order to achieve a small spot size. It is believed that intensity over 10 mW/μm^2 is required to realize optical recording at useful data rates[4]. Previous work on nano-aperture VCSELs has not been able to reach this requirement due to this rapidly decreased transmission efficiency of circular apertures with decreasing aperture size.

The transition towards research on unconventional apertures, or ridged apertures, coined after the ridge waveguides in microwave applications has spawned a new generation of VSCELs with the potential to realize the goal of strongly confined spot size and high enough intensity for high density optical recording. The C-, H-, I-, and bowtie-shaped shaped nano-apertures marked an increasing evolution towards high-intensity coherent light source with sub-100-nm near-field spot.

Using numerical finite-difference time-domain (FDTD) simulations, Xiaolei Shi discovered a unique non-symmetrical C-shaped nano-aperture (C-aperture) which can provide three orders of magnitude higher transmission efficiency than a square aperture with the same near-field spot size. The C-shaped aperture in a 120-nm-thick Ag film, designed for resonant transmission at a wavelength of 1 μm, can have a power throughput (defined as the ratio of aperture transmission cross section to aperture area) of 2.2 and a near-field spot size of 115×130 (nm). Further, they designed a scaled-up experiment at microwave frequencies which confirmed the simulation findings[9−11].

This discovery significantly relieves the difficulty of achieving high transmission through a conventional nano-aperture while maintaining strong near-field confinement. Thornton and Shi proposed the idea of applying the C-aperture onto VCSELs and reducing the number of top DBR in VCSELs to enhance transmission through the C-aperture[12]. However, they did not realize the C-aperture VCSEL experimentally because they did not address the problem of polarization control of VCSEL, which must be resolved in order to apply the highly polarization-sensitive C-aperture on VCSELs.

Jin *et al.* studied the transmission of nano-apertures in metal films deposited on a quartz substrate[13]. They used an illumination-collection-type near-field scanning optical microscopy (NSOM) to measure the near-field spots from a bowtie-aperture and compared that to rectangular and square apertures of the same area. The measured spot size from the bowtie-aperture which was found to be 65×34 (nm) is much smaller than that from the rectangular and square aperture, found to be 102×176 (nm) and 278×65 (nm), respectively. For the square aperture which was supposed to produce similar spot size to the bowtie-aperture, no observable spot was obtained due to the extremely low transmission efficiency through this square aperture[13].

Interestingly, the phenomenon of electromagnetic coupling to a surface electromagnetic wave propagating along a metal and dielectric interface was found to enhance transmission efficiency. It was shown that surface plasmons, also known as surface plasmon polaritons, can be excited in periodic arrays of sub-wavelength apertures in metal film; the coupling and re-radiation of surface-plasmons leads to largely enhanced transmission through the aperture arrays[14]. This work sparked increased research interests in exploiting surface plasmons to enhance transmission through sub-wavelength metal structures.

Hashizume and Koyama used a SiO$_2$-Au interface to study the effects of plasmons on the near field optical intensity of VSCELs. The SiO$_2$ layer was sandwiched between an upper gold layer with an 850-nm metal nanoaperture and a GaAs substrate. The excited surface plasmon increased the output intensity by more than a factor of sixteen. For a double aperture with SiO$_2$ layer, the measured intensity is 2.5 mW/μm^2. At the other extreme, a single aperture without the SiO$_2$ layer had an output of 0.19 mW/μm^2. This enhancement in power output comes with the added advantage of a small spot size: a 260-nm full-width at half-maximum (FWHM) with the SiO$_2$layer as opposed to 360 nm without the SiO$_2$ layer[7].

Insertion of the SiO$_2$ layer into the nano-aperture VCSEL structure enhances the transmission through the nano-aperture by three mechanisms. Firstly, insertion of the low-refractive-index SiO$_2$ layer reduces the reflection from the nano-aperture at the interface between the incident medium and air, which is given by

$$\frac{E_{\text{reflected}}}{E_{\text{incident}}} = \frac{n_{\text{incident}} - n_{\text{air}}}{n_{\text{incident}} + n_{\text{air}}}. \qquad (3)$$

Without the SiO$_2$ layer, n_{incident} becomes the high-refractive index of AlGaAs, leading to a high reflection. With the SiO$_2$ layer, n_{incident} becomes the low-refractive index of SiO$_2$, which largely reduces the reflection. Secondly, a Fabry-Perot resonance can build up inside the SiO$_2$ layer, which increases the intensity incident onto the nano-aperture. Thirdly, insertion of the SiO$_2$ layer significantly changes the spectral response for a given nano-aperture, as shown in the spectral response of the C-aperture in Fig. 2.

Continued studies on plasmon effects as well as incorporating novel materials onto VSCELs proved to be essential to improving transmission efficiency. Using noble metals, such as Au, have been known to increase the transmission efficiency in nano-aperture VSCELs. Au bowtie antennae fabricated with e-beam lithography have been shown to have greatly enhanced intensity and field confinement[15].

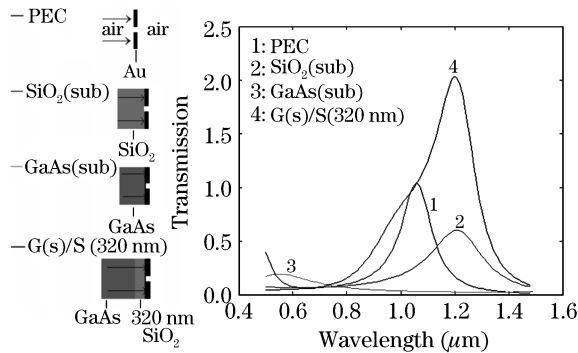Also, it was discovered that plasmon enhancement using a metal nano-particle increased the output power.

Fig. 2. Transmission spectrum through a C-aperture with different materials as incident medium (PEC stands for perfect electrical conductor).

The addition of a 100-nm-diameter Au nano-particle situated at the center of a 400-nm-diameter aperture revealed a 1.8 times power enhancement to about 0.36 mW at 5 mA drive current. Also, this design was operational at a low threshold current of less than 300 μA which may be advantageous for novel nano scanning probe tools[5].

More recently, implementation of a Au bowtie nano-aperture, the complement of the bowtie antennae, onto VCSELs, yielded a spot size of 64×66 (nm) at 20 nm away. Simulation results indicate a near-field intensity of up to 47 mW/μm^2[16].

3. Nano-aperture VSCEL design and fabrication

The top-emitting VCSELs were designed to operate at 972 nm and consisted of 38.5 pairs of n-type Al$_{0.08}$Ga$_{0.92}$As/Al$_{0.92}$Ga$_{0.08}$As DBR, three In-GaAs/GaAsP quantum wells (QWs), and 9.5 pairs of p-type Al$_{0.08}$Ga$_{0.92}$As/Al$_{0.92}$Ga$_{0.08}$As DBRs[16]. The number of top p-type DBR pairs is only about one third of that in a conventional VCSEL, which is designed to increase the intensity incident onto the nano-aperture. The reflectivity of the top mirror is enhanced with a 150-nm-thick Au coating. A half-wavelength thick SiO$_2$ film is inserted between the Au coating and the top DBR mirror to enhance the transmission through the nano-aperture. Here $\lambda/(2 \times n_{SiO_2}) = 972/(2 \times 1.5) = 324$ nm, where n_{SiO_2} is the refractive index of SiO$_2$ at a wavelength of 972 nm. The thickness of a half-wavelength thick SiO$_2$ film is 324 nm. The nano-apertures are etched through the Au coating using a Ga$^+$ FIB. The nano-aperture needs to be placed in the center of the top mesa, which can be easily located in the lithographically defined circular mesa. This is far easier for the VCSEL compared to the EEL where the nano-aperture requires a precise alignment with the QW region which is buried under the facet coatings and is hard to locate. Figure 3 shows a schematic structure of the nano-aperture VCSEL.

Wet oxidation of Al$_{0.98}$Ga$_{0.02}$As is used to obtain a 2.8-μm-diameter oxide aperture for current and mode confinement. This particular size of oxide aperture was chosen as a tradeoff between the optical mode area and the roll-over current. As noted before, a smaller oxide aperture leads to a smaller optical mode area and hence can increase the quantum efficiency of nano-aperture VCSELs. However, if the oxide aperture is too small, the rollover current, which is the current beyond which the power output from the laser starts to decrease with
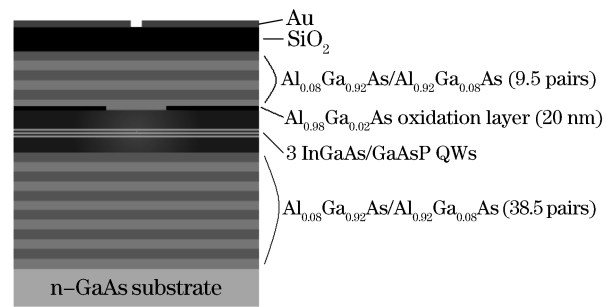

Fig. 3. Nano-aperture VCSEL structure.

increasing injection current due to excessive heating, decreases significantly. This limits the maximum output power that can be achieved with the nano-aperture VCSEL.

Although the number of DBR pairs in the top mirror of the nano-aperture VCSEL structure is only one third of that in conventional VCSELs, the reflectivity of the top mirror combination is enhanced by the Au coating and is comparable to that in conventional VCSELs. The bottom mirror consists of 38.5 pairs of DBRs and is similar to that in conventional VCSELs.

One of the most important issues in designing this VCSEL structure is the phase matching condition. For the VCSEL to laze at the designed wavelength, the round trip phase for a photon must be precisely equal to an integer number of 2π. In a conventional VCSEL, this condition is satisfied by designing the optical thickness of the laser cavity to be an integer number of half wavelengths. In our VCSEL structure, an additional Au coating is used to enhance the reflectivity of the top mirror. However, the reflection from the Au layer causes some additional phase shift. A special AlGaAs layer is used as part of the last DBR layer to provide phase matching to compensate for this phase shift. Under this phase matched condition, the peak of the standing wave pattern exactly overlaps the three QWs, as shown in Fig. 4, and thus satisfies the lasing condition.

The fabrication process flow for the nano-aperture VCSEL is shown in Fig. 5. First, a half-wavelength thick SiO$_2$ layer is deposited onto the VCSEL wafer by sputtering. A SiO$_2$ mesa is then defined by a combination of dry and wet etching. Then the top ring contact is
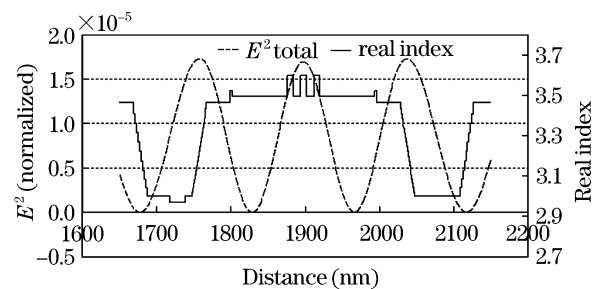

Fig. 4. E^2 distribution of the standing wave inside the laser cavity. Real part of the refractive index of each layer is shown by the solid line. The distance in x-axis starts from the topmost layer of the VCSEL epitaxial structure. E^2 stands for the square of electric field and is proportional to the light intensity.

1) deposit SiO$_2$ layer and define SiO$_2$ mesa

2) deposit top contact and define top mesa

3) deposit bottom contact

4) oxidation for mode confinement

5) planarize with photoresist

6) deposit planar contact

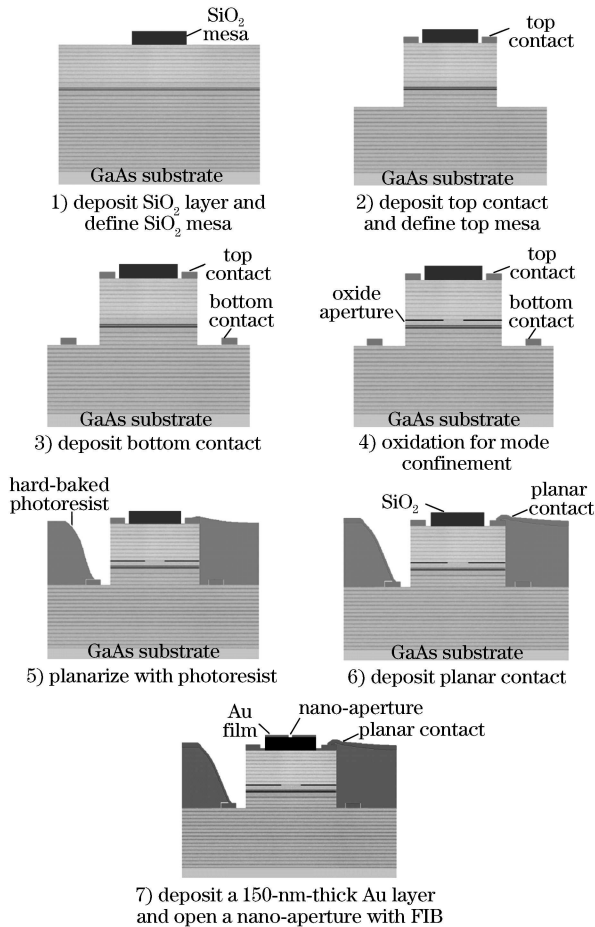7) deposit a 150-nm-thick Au layer and open a nano-aperture with FIB

Fig. 5. Processing flow of the nano-aperture VCSELs.

deposited and the top mesa is defined by dry etching. Next, a bottom ring contact is deposited. Then wet oxidation of AlGaAs is done to form an oxide aperture for current and optical mode confinement. After oxidation, the structure is planarized with photoresist. Next, a planar contact is deposited to connect to the top and bottom ring contact. Finally, a 150-nm-thick Au film is deposited and patterned on top of the SiO$_2$ layer. A nano-aperture can then be etched in the metal film using a FIB to obtain a nano-aperture VCSEL.

Figure 6 shows an optical microscope image of the top view of the processed VCSEL before opening a nano-aperture.

Among all the processing steps for the nano-aperture VCSEl, control of the oxidation of AlGaAs to form an oxide aperture is especially important. We need to start
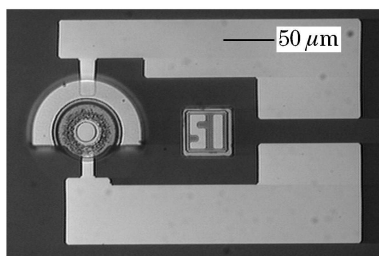

Fig. 6. Optical microscope image of the top view of the fabricated VCSEL before opening a nano-aperture.

with a mesa of about 40-μm diameter, and subsequently, obtain an oxide aperture of about 3-μm diameter to ensure single-transverse-mode lasing. A wet oxidation system with in-situ monitoring was developed in our group. With this capability of in-situ monitoring, the
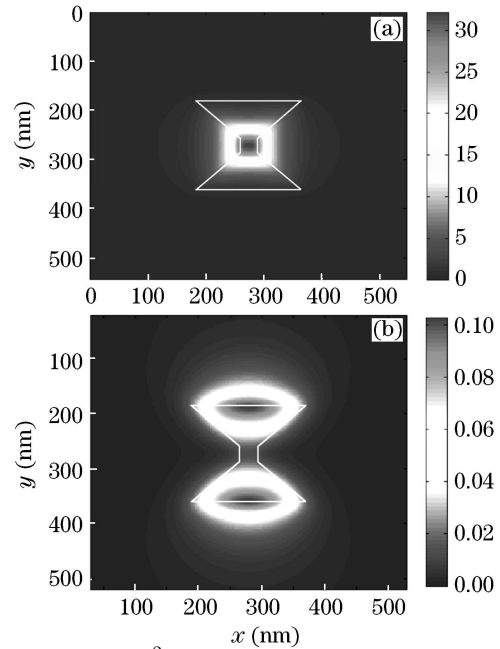

Fig. 7. Near-field E^2 distribution at 20 nm away from the bowtie-aperture. (a) The polarization is along x-direction; (b) the polarization is along y-direction.
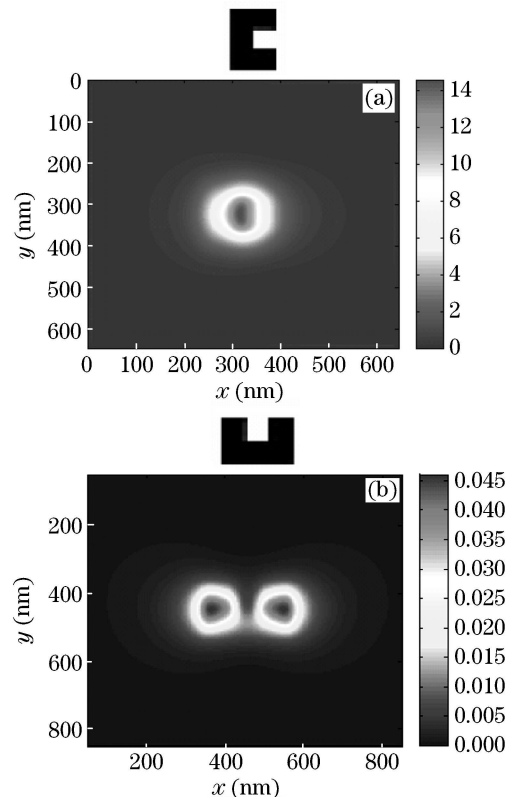

Fig. 8. Near-field E^2 distribution at 30 nm away from the C-aperture. (a) the polarization is along x-direction and perpendicular to the height of the C-aperture above the figure; (b) the polarization is along x-direction and parallel to the height of the C-aperture above the figure.
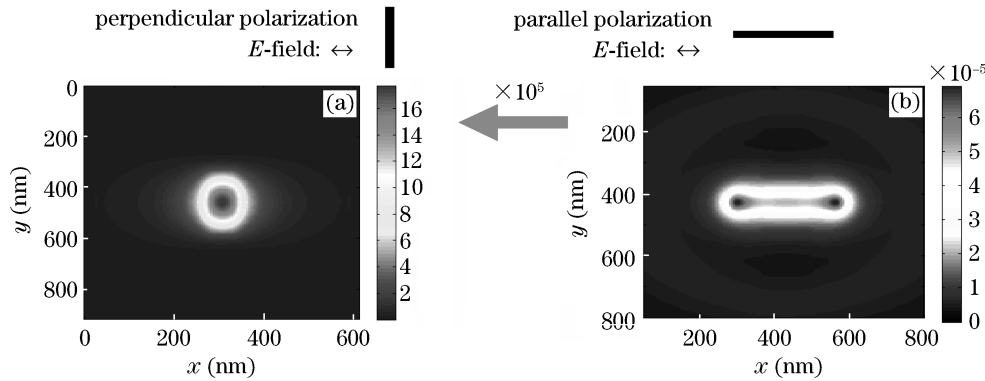
Fig. 9. E^2 distribution from a 50×280 (nm) slit under different polarization. (a) The polarization is perpendicular to the slit; (b) the polarization is parallel to the slit.

oxidation process can now be easily stopped when the desired oxide aperture size is reached.

4. VCSEL polarization control

The transmission of light through the ridge apertures is highly polarization-dependent. For example, for the bowtie-aperture, when incident light is polarized along the two metal tips, a well-confined near-field spot with high intensity was produced, as shown in Fig. 7(a). In contrast, the orthogonal polarization results in a poorly confined near-field spot and the intensity was three hundred times lower, as shown in Fig. 7(b).

The C-aperture, H-aperture, and I-aperture all have similar polarization-dependent transmission properties. For example, for the C-aperture, the intensity is over three hundred times higher and the spot size is much smaller for the desired polarization than that for the mismatched polarization, as shown in Fig. 8. Thus, in order to obtain high power transmission and strong near-field confinement from these ridge nano-apertures, the polarization of the incident light must be controlled to be along the desired direction.

A number of efforts have been attempted to improve polarization stability of VCSELs. Overall, these approaches can be classified into two categories. The first is to introduce a difference in loss for the two polarization states, including utilizing an asymmetrical mesa structure[17], using external optical feedback from polarization sensitive gratings[18], opening rectangular metal aperture arrays[19] or integrating a subwavelength grating as the top mirror[20] etc. The second method is to introduce a gain difference for the two polarization eigenstates, which includes growing on $\langle n11 \rangle$ (where $n \leq 3$) oriented substrates[21], by means of asymmetric current injection[22], or using external strain induced by a stressor[23]. In the ridge nano-aperture VCSELs, the polarization selection mechanism must be strong enough to dominate over the polarization selectivity of the ridge apertures.

A novel integrated solution to control the polarization by opening narrow slits (50×1500 (nm)) in the Au film surrounding the ridge nano-aperture using the FIB has been developed[24]. For slits with width much smaller than one wavelength, only the mode with polarization perpendicular to the slits can propagate through.

Thus the slits have high transmission selectivity over the two orthogonal polarizations. The structure of the slits is further optimized to improve their polarization selectivity[25]. The slit width is fixed at 50 nm and the slit length is tuned via FDTD simulation until transmission resonance occurs at the lasing wavelength for light polarized perpendicular to the slit. An optimized slit length of 280 nm is chosen. Figures 9(a) and (b) show the near-field E^2 distribution of a 50×280 (nm) slit under incident light of the lasing wavelength (i.e., around 972 nm) with polarization perpendicular and parallel to the slit respectively. The optical power for the perpendicular polarization is five orders of magnitude higher than that for the parallel polarization. Thus the perpendicular polarization state has higher loss due to higher transmission through the slits and the polarization of the VCSELs should be pinned parallel to the slit.
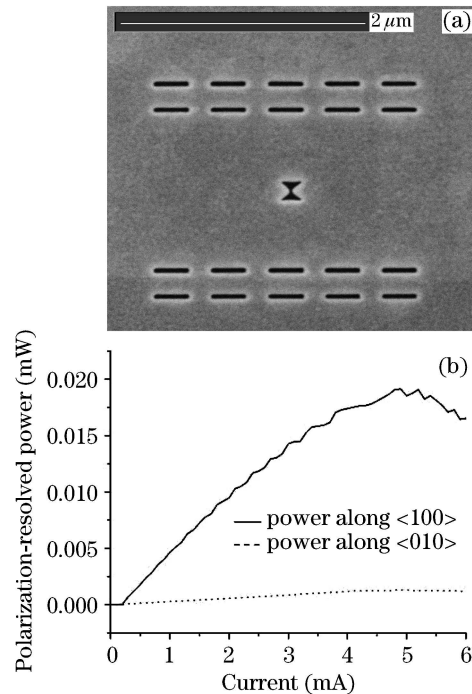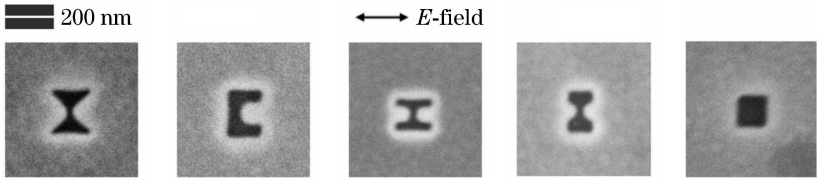

Fig. 10. (a) Scanning electron microscope image of twenty 50×280 (nm) slits and a bowtie-aperture; (b) polarization-resolved power emitted through the substrate of a VCSEL with twenty 50×280 (nm) slits oriented along $\langle 100 \rangle$ direction.

Table 1. Comparison of Nano-Aperture VCSELs Using Bowtie-Aperture, C-Aperture, H-Aperture, I-Aperture, and Square Aperture[a]

	Bowtie-Aperture	C-Aperture	H-Aperture	I-Aperture	Square Aperture
Aperture Area ($\times 10^4$ nm^2)	1.67	2.65	1.80	1.69	1.69
Spot Size 20-nm Away (nm)	64×66	72×104	82×68	64×68	174×100
Far-Field Power (μW)	188	157	94	162	12
Near-Field Intensity (mW/μm^2)	47	25	18	43	0.8

[a]The controlled polarization direction of the incident light is shown above the SEM images of the apertures.

Twenty 50×280 (nm) slits are opened in the Au coating along the $\langle 100 \rangle$ direction as shown in Fig. 10(a). The slits are separated in two groups spaced by 1500 nm to leave enough modal area to add the ridge aperture, such as a bowtie-aperture as shown in Fig. 10(a). The slits in each group have a pitch of 250 nm in both horizontal and vertical directions. Figure 10(b) shows the polarization-resolved bottom-emitting power from a VCSEL with twenty 50×280 (nm) slits. It can be seen that the polarization of the VCSEL is effectively controlled to be along $\langle 100 \rangle$ direction, namely, parallel to the slits.

5. Ridge nano-aperture VCSELs

With the VCSEL polarization controlled by the above mentioned nano-slits, the polarization-sensitive ridge nano-apertures can now be applied to the VCSEL. The measured total far-field power, estimated near-field FWHM intensity spot size 20 nm away from the ridge apertures, and the corresponding near-field intensities from VCSELs using different ridge apertures including bowtie, C-, H-, and I-apertures are summarized in Table 1[26]. A 130-nm square aperture with about the same area as the bowtie-aperture is also listed for comparison. All the ridge apertures show strong transmission enhancement over the 130-nm square aperture. Also, note that the near-field spot size from the 130-nm square aperture is much larger than those from the ridge apertures. Experimental comparison with square apertures producing the same spot size as the ridge apertures is unachievable due to the extremely low and undetectable power output from a sub-100-nm square aperture VCSEL.

In comparison amongst the different ridge apertures, the bowtie-aperture VCSEL shows the highest intensity and smallest spot size, which may be attributed to the additional lightning rod effect from the sharp tips of the bowtie-aperture. The C-aperture design may be further optimized to achieve smaller spot size and higher intensity by shrinking the aperture size and tuning the structure[11,27], although the smaller aperture size can add to the challenge for fabrication. The relatively lower power output from the H-aperture may be due to fabrication imperfection with the FIB, such as rounding at the corners and tapering from the etching, because of its smaller feature size.

6. Conclusion and Future Directions

Although direct measurement of the near-field spot size from the ridge apertures on VCSELs has not been accomplished, the strong near-field confinement of the ridge apertures has been demonstrated experimentally. Chen et al. measured a near-field spot size of 90×70 (nm) from a C-aperture on an EEL[28]. And Jin et al. measured a near-field spot size of 106×80 (nm) from an H-aperture[29]. The bowtie-aperture[30] and C-aperture[31] have also been applied in contact optical lithography, in which the high resolution of these apertures was demonstrated. These near-field experiments indicate that the measured near-field confinement of ridge apertures agrees with the simulation results.

Thus, in the attempt to achieve a smaller spot size with greater power density, we have progressed from EEL to VCSELs with circular, square, C-shaped, H-shaped, I-shaped, and bowtie-shaped nano-apertures. The continual progress of pushing the fabrication limits of very small features, overcoming the limitations of far-field optics, and achieving confined near-field intensity will shape the technology and the applications that rely on nano-scale optical precision. Indeed, engineering progresses in the field of nano-aperture VSCELs has accelerated during the past ten years, with simulations and theoretical calculations being supported by experimental data. Future work includes, and is in no way limited to, experimentally demonstrating the extrapolated near-field intensity, the possibility of redefining the active QW region into quantum dots, and demonstrating many applications of high-intensity ridge nano-aperture VCSELs, such as ultrahigh-density near-field optical data storage or high-resolution near-field imaging. It is clear that because of their combination of high efficiency, high power, low cost, and 2D array capabilities, nano-aperture VCSELs can provide a foundation to realize many new sub-wavelength near field optical systems and applications.

Z. Rao's e-mail address is zhilongrao@gmail.com.

References

1. A. Partovi, D. Peale, M. Wuttig, C. A. Murray, G. Zydzik, L. Hopkins, K. Baldwin, W. S. Hobson, J. Wynn, J.

Lopata, L. Dhar, R. Chichester, and J. H.-J. Yeh, Appl. Phys. Lett. **75,** 1515 (1999).

2. Y.-J. Kim, K. Suzuki, and K. Goto, Jpn. J. Appl. Phys. **40,** 1783 (2001).

3. R. L. Thronton and L. Hesselink, "Near-field laser and detector apparatus and method" US patent 6574257 (June 2003).

4. S. Shinada, F. Koyama, N. Nishiyama, M. Arai, and K. Iga, IEEE J. Sel. Top. Quantum Electron. **7,** 365 (2001).

5. J. Hashizume and F. Koyama, Appl. Phys. Lett. **84,** 3226 (2004).

6. J. Hashizume, P. B. Dayal, and F. Koyama, *IEEE 20th International Semiconductor Laser Conference* 101 (2006).

7. J. Hashizume and F. Koyama, Opt. Express **12,** 6391 (2004).

8. H. A. Bethe, Phys. Rev. **66,** 163 (1944).

9. X. Shi, L. Hesselink, and R. L. Thornton, Opt. Lett. **28,** 1320 (2003).

10. X. Shi and L. Hesselink, Jpn. J. Appl. Phys. **41,** 1632 (2002).

11. X. Shi, "Resonant optical transmission through a single sub-wavelength aperture for near-field applications" Ph. D. Thesis (University of Stanford, 2003).

12. R. L. Thornton and X. Shi, "Near field optical apparatus", US patent 7095767 (August 2006).

13. E. X. Jin and X. Xu, Appl. Phys. Lett. **88,** 153110 (2006).

14. T. W. Ebbesen, H. J. Lezec, H. F. Ghaemi, T. Thio, and P. A. Wolff, Nature **391,** 667 (1998).

15. P. J. Schuck, D. P. Fromm, A. Sundaramurthy, G. S. Kino, and W. E. Moerner, Phys. Rev. Lett. **94,** 017402 (2005).

16. Z. Rao, L. Hesselink, and J. S. Harris, Opt. Lett. **32,** 1995 (2007).

17. T. Yoshikawa, H. Kosaka, K. Kurihara, M. Kajita, Y.

18. S. J. Schablitsky, L. Zhuang, R. C. Shi, and S. Y. Chou, Appl. Phys. Lett. **69,** 7 (1996).

19. J. Hashizume, P. B. Dayal, and F. Koyama, *IEEE 20th International Semiconductor Laser Conference* 101 (2006).

20. M. C. Y. Huang, Y. Zhou, and C. J. Chang-Hasnain, Nature Photon. **1,** 119 (2007).

21. M. Takahashi, P. Vaccaro, K. Fujita, T. Watanabe, T. Mukaihara, F. Koyama, and K. Iga, IEEE Photon. Technol. Lett. **8,** 737 (1996).

22. L. M. Augustin, E. Smalbrugge, K. D. Choquette, F. Karouta, R. C. Strijbos, G. Verschaffelt, E.-J. Geluk, T. G. van de Roer, and H. Thienpont, IEEE Photon. Technol. Lett. **16,** 708 (2004).

23. Y. Matsui, D. Vakhshoori, P. Wang, P. Chen, C. Lu, M. Jiang, K. Knopp, S. Burroughs, and P. Tayebati, IEEE J. Quantum Electron. **39,** 1037 (2003).

24. Z. Rao, J. A. Matteo, L. Hesselink, and J. S. Harris, Proc. SPIE **6132,** 61320J (2006).

25. Z. Rao, J. A. Matteo, L. Hesselink, and J. S. Harris, Appl. Phys. Lett. **90,** 191110 (2007).

26. Z. Rao, L. Hesselink, and J. S. Harris, Opt. Express **15,** 10427 (2007).

27. X. Shi, L. Hesselink, and R. L. Thornton, Opt. Lett. **28,** 1320 (2003).

28. F. Chen, A. Itagi, J. A. Bain, D. D. Stancil, T. E. Schlesinger, L. Stebounova, G. C. Walker, and B. B. Akhremitchev, Appl. Phys. Lett. **83,** 3245 (2003).

29. E. X. Jin and X. Xu, J. Heat Transfer **129,** 37 (2007).

30. L. Wang, S. M. Uppuluri, E. X. Jin, and X. Xu, Nano Lett. **6,** 361 (2006).

31. L. Wang, E. X. Jin, S. M. Uppuluri, and X. Xu, Opt. Express **14,** 9902 (2006).

Sugimoto, and K. Kasahara, Appl. Phys. Lett. **66,** 908 (1995).